Radiation Belts

Paul Bühler (paul.buehler@psi.ch)
Paul Scherrer Institute, CH–5232 Villigen PSI, Switzerland

Abstract

The earth's radiation belts consist of energetic electrons and ions which are trapped in the earth's magnetic field. However, there are various physical processes, losses and sources, which alter the trapping mechanism. The radiation belts are therefor not a stable structure but are rather to be understood as the result of a dynamic interplay of various acting processes. The variability of the belts, which is a subject of "Space Weather", is driven by the temporal variations of the involved ingredients. In this paper various different kinds of radiation belt variations are presented and the involved physical processes are discussed.

1. Introduction

The radiation environment of the inner magnetosphere, which is the region of space periodically passed by most of the commercial and scientific satellites, is dominated by high energetic charged particles, trapped in the earth's magnetic field. These particles, electrons with energies above a few hundred keV and protons with energies exceeding a few MeV, form a potential danger to spacecrafts. They can penetrate several millimeters of shielding material and reach sensitive components, where the energy deposit can leed to various, from disturbing to disastrous effects (see Effects and Users section of this issue).

The average structure of the radiation belts, as described by the widely used AE8/AP8 models from NASA [*Vette, 1991, Sawyer & Vette, 1976*] is shown in figure 1. The left panel shows integral flux level contours of >10 MeV protons, and the right panel, contours of the >0.6 MeV electrons. There are two main zones which are populated by trapped particles, the inner radiation belt, centered at around 1.5 R_E (earth radius R_E) and the outer radiation belt, centered at approximately 4 R_E. Whereas protons are restricted to the inner belt, electrons can be found in both regions. The zone between the two belts is the so-called slot region. Except that there exists two sets of the AE8/AP8 models, one for solar minimum and one for solar maximum, they are static. The models suggest the radiation belts to be a stable structure, which is not the case. The trapped particle population is subject to temporal variations with a wide range of characteristic time scales, reaching from solar cycle variations to changes which take place within minutes and are initiated by solar events.

The purpose of this paper is to review the most apparent variations of the radiation belts and discuss involved physical processes. In section 2 the trapping of charged particles in the earth's magnetic field is discussed. Variations of the proton belt are presented in section 3, whereas the variations of the electron belts are addressed in section 4.

2. Trapping of charged particles in the earth's magnetic field

The movement of a charged particle with charge q and mass m in an electromagnetic field is described by equation (1)

$$m\frac{d^2\underline{r}}{dt^2} = q\frac{d\underline{r}}{dt} \wedge \underline{B} + q\underline{E} + \underline{F} \qquad (1)$$

where the additional forces $\underline{F}$ include gravitation.

In a non trivial electromagnetic field configuration, like the one present in the magnetosphere, the trajectories can be very complicated [*Stoermer, 1907*]. Under the assumption that the radius of gyration of the particle is small compared to the field gradients and the electric field term in equation (1) is small compared to the magnetic term, the movement of the particle can be described by the so called guiding center approximation [*Northrop & Teller, 1960*]. The particle trajectory is expressed as $\underline{r} = \underline{R} + \underline{\rho}$, where $\underline{R}$ denotes the trajectory of the center of gyration, the guiding center, and $\underline{\rho}$, the position of the particle with respect to the guiding center. As a result of this approximation it turns out that the motion of the guiding center can be expressed as a motion along field lines and a drift motion perpendicular to the magnetic field lines. In the earth's dipole like magnetic field, where the magnetic field strength increases with increasing magnetic latitude, there exist points in the northern and southern hemisphere, the so-called mirror points (M_1 and M_2), where the particles traveling along a field line are reflected, leading to a bouncing along the field lines between the conjugate points. The motion perpendicular to the field lines causes a drift around the earth, which is eastward for electrons and westward for protons. Thus the motion of a trapped particle is defined by three

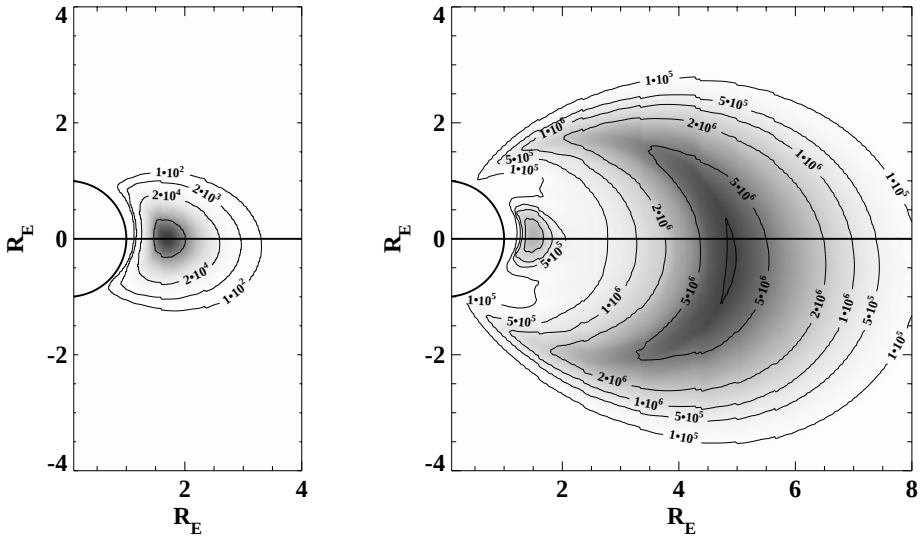

Figure 1: Earth's radiation belts as represented by the standard AE8 and AP8 models. The two panels show contour plots of integral fluxes of (left) protons with energies E > 10 MeV and (right) electrons with energies E > 0.6 MeV. Whereas electrons populate the inner and outer zone, protons are only trapped in the inner zone.

cyclic motions, gyration, bounce along field lines, and drift around the earth.

To each of these cyclic motions an adiabatic invariant can be associated. They are denoted by μ (first invariant, gyration), J (second invariant, bouncing), and Φ (third invariant, drift). Their definitions are given in equation (3). The motion of the guiding centers describe shell like surfaces around the earth, which are defined by the adiabatic invariants. By combining the three invariants to a single parameter, the so-called L-shell parameter, L, the class of particles moving on the same shell can be addressed by a single value [*McIlwain, 1961*]. L has the dimension of a length and is usually given in earth radii. In a first approximation it can be thought of as the radial distance of the shell-equator crossing point.

$$\begin{aligned} \mu &= \frac{p_\perp^2}{2m_0 B} \propto \frac{sin^2(\alpha)}{B} \\ J &= \int_{M_1}^{M_2} p_\parallel ds \\ \Phi &= \oint \underline{B} dF \end{aligned} \qquad (2)$$

$p_\perp$ and $p_\parallel$ are the components of the particle's momentum perpendicular and parallel to the local field line. Conservation of energy and first invariant causes the pitch angle α (angle between particle trajectory and local magnetic field line) to increase as the guiding center moves along the field line to higher magnetic latitudes, where the magnetic field B becomes stronger. The mirror points are defined by the locations, where α reaches 90°. The locations of the mirror points are independent of the particle energy and are solely a function of the magnetic field configuration and the equatorial pitch angle, α_0. Φ is the flux of the magnetic field enclosed by the surface J=constant.

The adiabatic invariants are constants of motion as long as the temporal variations of the acting forces are slow compared to the respective periods of motion. The periods depend on particle species, energy and magnetic field strength. Typical values for particles trapped in the heart of the inner and outer belt are given in table 1.

Table 1: Typical periods for particles trapped in the inner and outer belt region.

	Periods [sec]			
	p, 100 MeV		e^-, 1 MeV	
	L=1.5	L=4.5	L=1.5	L=4.5
Gyration	10^{-2}	10^{-1}	10^{-5}	$3 \cdot 10^{-4}$
Bouncing	0.25	0.5	0.1	0.3
Drift	30	10	3000	1000

Since the period of the drift motion is largest, the third adiabatic invariant risks first to be violated. Violation of the third invariant leads to radial diffusion [*Schulz & Lanzerotti, 1974*]. The particles diffuse in- or outward in L-space, depending on the radial gradient of the phase-space density distribution. Violation can be caused by fluctuations of the electric (electric diffusion) or magnetic (magnetic diffusion) field. Inward diffusion under conservation of the first invariant leads to an acceleration of the particle, as it moves to regions with stronger magnetic field and vice versa outward diffusion to deceleration. Violation of the first two invariants causes changes of the pitch angle (pitch angle scattering). This can lead

to losses of particles, when the pitch angle becomes so small, that the corresponding mirror points move down into the atmosphere where the particles can be absorbed. As the periods of the first two invariants are short their violation is mainly caused by particle-particle and particle-wave interactions.

Although adiabatic changes conserve the adiabatic invariants, they cause changes of the observed particle distributions. An adiabatic magnetic field decrease leads to a deceleration (conservation of first invariant) and outward motion of the L-shell surface (conservation of third invariant). The changes however are reversible when the magnetic field recovers to its initial state.

The so far described trapping mechanism provides the basis for the existence of the radiation belts. However, there are additional sources and loss mechanisms which alter the trapping and must be considered in order to described the observed variations.

3. Protons

3.1 Protons in the inner belt region

The main source for the protons trapped in the inner radiation belt is the so-called Cosmic Ray Albedo Neutron Decay, CRAND [*Albert et al, 1998* and references therein]. The interaction of cosmic rays with constituents of the earth's atmosphere produce neutrons by spallation, which by chance are emitted into the trapping region. The beta decay of these neutrons produce protons which can become trapped. On the other hand the interaction of trapped protons with plasmaspheric and atmospheric particles, by charge exchange and coulomb collision, leads to losses of particles from stable trapping. The time scales of the losses and radial diffusion for high energy protons are of the order of years, such that the inner belt can be expected to be very stable, which indeed is the case.

However, solar cycle variations of the sources and losses lead to long-term variations of the trapped proton population. During solar maximum the cosmic ray flux reaching the earth is low compared to solar minimum, because of the shielding effect of the enhanced solar activity, thus the source low. The density of the upper atmosphere, is enhanced during solar maximum because of the enhanced solar heating. This leads to an enhanced absorption of protons in the upper atmosphere during solar maximum, thus a strong loss. The combination of these two effects leads to a solar cycle variation of the proton flux levels in the inner radiation belt, with high fluxes observed during solar minimum and low fluxes, during solar maximum. This is illustrated in figure 2, where proton fluxes of the inner belt, measured with instruments aboard the TIROS/NOAA weather satellites [*Huston & Pfitzer, 1998*] are plotted as function of time over a period of two solar cycles. The symbols, connected by solid lines show the > 80 MeV proton fluxes at different L-values. The dotted line shows $F_{10.7}$, the solar radio flux, which is used here as proxy for the solar heating of the earth's atmosphere. The solar cycle variation is most pronounced at low L-values, where the influence of the atmosphere is most important.

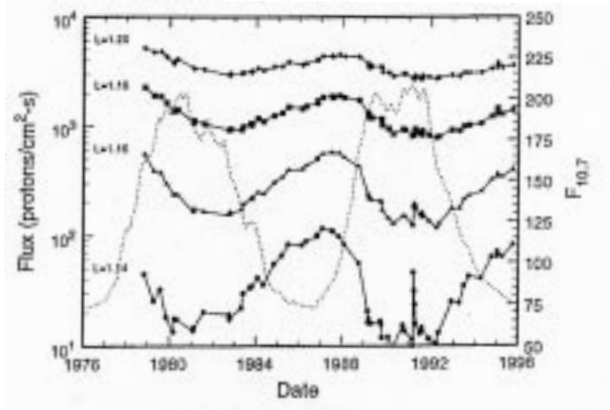

Figure 2: Flux of protons with energy > 80 MeV at the geomagnetic equator as function of time. The dotted line shows $F_{10.7}$. The solar cycle variations are most pronounced at small L-values (from Huston & Pfitzer [1998])

South Atlantic Anomaly

The South Atlantic Anomaly, SAA, is a feature of the inner radiation belt. Due to the shift and tilt of the earth's magnetic field dipole axes with respect to the earth's rotation axis, the earth's magnetic field has a local minimum centered in the South Atlantic. Trapped particles from the inner belt can reach there low altitudes. The location of the SAA depends on the magnetic field and thus drifts slowly with the secular drift of the magnetic field. Figure 3 shows the SAA as observed in 1996 aboard the Russian space station Mir [*Bühler et al., 1996*]. The upper panel shows a grey-scale map of the average dose rate measured behind a shielding of 2.06 g/cm^2 and the lower panel shows a horizontal cut through the map at a latitude of -32°. The dose rate peak position is located at approximately -43° longitude. The AE8/AP8 models predict the maximum in 1970 to be located at -36°. This corresponds to a yearly westward drift rate of approximately 0.27° per year.

The altitude gradient of the atmospheric density in the SAA causes an anisotropy of the trapped particle fluxes. At a given point the guiding centers of protons moving from west to east are located below that point, whereas the guiding centers of protons moving from east to west are located above that point. Therefore particles coming from west experi-

ence denser regions of the atmosphere and are more absorbed [*Lencheck & Singer, 1962*]. The effect is most important at high energies, where gyroradii are large and therefore the difference in altitude of the guiding centers is big. Aboard Mir an east-west ratio of a factor 4 at 200 MeV has been measured [*Bühler et al, 1998a*] in the SAA. As the anisotropy is linked to the atmospheric density a solar cycle dependence can be expected.

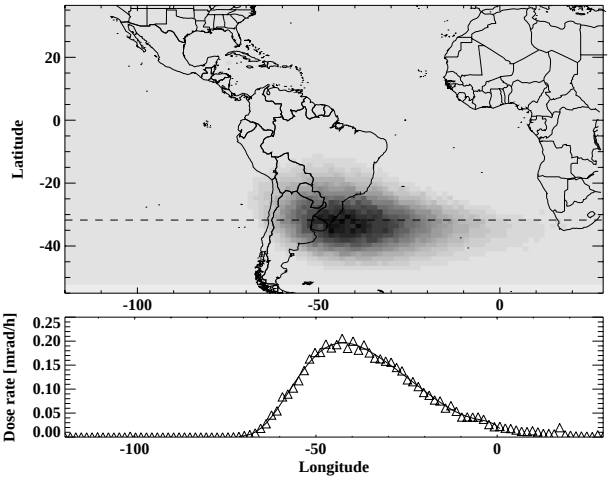

Figure 3: Dose rate map measured during 1996 aboard Mir. The lower panel shows a longitudinal profile at -32° latitude. The position of the SAA is subjected to a secular drift. The measured position of the maximum dose rate in 1996 is -43° longitude. This is roughly 7° more east than the AE8/AP8 models predict for 1970, which corresponds to a shift rate of 0.27° per year.

3.2 Protons in the outer belt region

Normally the high energy proton flux in the outer belt region is very small. But protons emitted from the sun during solar proton events, Solar Energetic Particles, SEP, can penetrate into the inner magnetosphere and form short-lived radiation belts [*Gussenhoven et al., 1994*]. Figure 4 shows an example. In the lower panel the flux of protons with energies of approximately 50 MeV measured aboard GOES at geosynchronous orbit, GEO are plotted as function of time. In the evening of October 19, 1994 a sudden increase by almost a factor 100 within a few hours was registered. The upper three panels show 35 MeV protons for the same period but as function of the L-shell parameter measured aboard STRV-1b in an equatorial geosynchronous transfer orbit, GTO. Before the increase at GEO the GTO proton rates are at background level in the outer belt zone. The increase below L=3 is due to the inner belt. During the proton enhancement at GEO the GTO rates are enhanced down to approximately L=4 R_E. But they decay together with the fluxes measured at GEO. The penetration of solar protons at these energies deep into the magnetosphere is not expected because of the shielding effect of the earth's magnetic field. However, such events are always associated with magnetic field disturbances, which can alter the shielding effect or even accelerate particles and carry them to low L-values [*Hudson et al., 1998*]

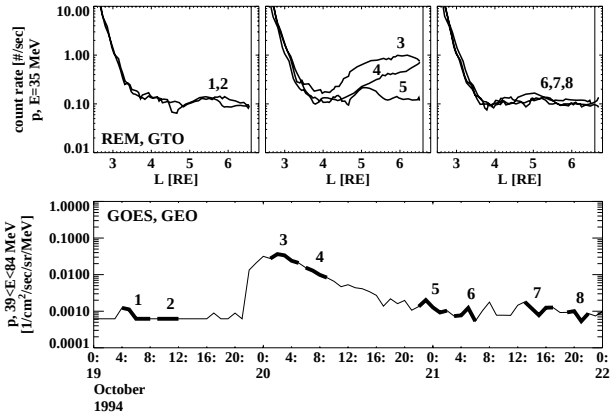

Figure 4: High energetic protons observed at GEO and GTO during a Solar Particle Event. In the lower panel the 50 MeV proton flux measured at GEO is plotted versus time, whereas the upper three panels show radial proton profiles measured in GTO at different times. The protons temporarily penetrate down to $L \approx 4$ but do not remain trapped for a long time.

4. Electrons

In contrary to the high energy protons, electrons are trapped in the inner and outer zone. The two zone structure is a consequence of radial diffusion and steady losses [*Lyons and Thorne, 1973*]. In the outer zone the electron losses are dominated by pitch-angle scattering due to wave-particle interactions, whereas in the inner zone the trapping lifetime is limited by coulomb scattering. The time scales of diffusion and losses depend on energy and L-value and range from few days at large L and low energies to month and years for high energetic electrons in the inner zone. Figure 5 shows data obtained with an instrument in GTO for a long lasting geomagnetically quiet period, and demonstrates the inward motion and decay of the trapped electron population in the outer radiation belt. We will see later (section 4.2), that during geomagnetically active periods the behavior of the outer belt electrons is considerably different. The upper panel shows the position of the maximum electron rate in L, L_{max} and the lower panel, the maximum rate (asterisks). From April 20, 1996 on, when the electron rates reached a maximum, the outer belt steadily decaied and the maximum of the L-distribution moved to lower L-values over a period of four month. Decay rate and inward motion are

a function of L. Using data from the POLAR satellite Selesnick et al. [1997] found that a decay rate $\propto (L/4)^8$ and a diffusion constant $D_{LL} \propto (L/4)^{10}$ does best fit the observations. Towards the end of the period, secondary peaks appeared at large L-values (diamonds). Inner and outer peaks coexisted until the outer part had grown and swamped the inner peak.

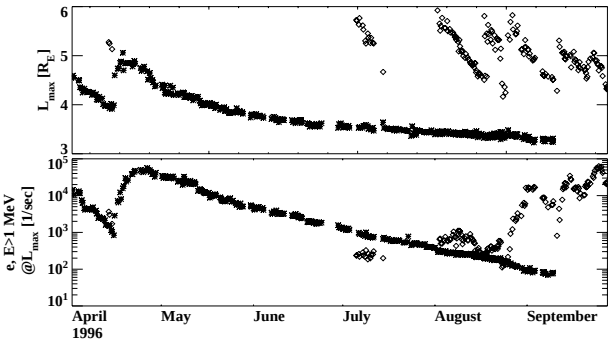

Figure 5: Decay and inward motion of the electron distribution during a geomagnetically quiet period observed in GTO. The upper panel shows the L-value at which the radial count rate profile peaked and the lower panel shows the peak rate (asterisks) as function of time.

4.1 Electrons in the inner belt region

Similar to the inner belt protons the inner belt electrons exhibit a solar-cycle variation. But whereas in the case of the protons the source and loss vary synchronously with the solar-cycle (high source, low losses during solar minimum, and vice versa during solar maximum), they are varying asynchronously for the electrons [*Abel et al., 1994*]. During solar maximum the outer belt, source of the inner belt electrons, as well as the losses into the atmosphere, can be expected to be enhanced compared to solar minimum. This can lead to the situation shown in figure 6, where there are two parts of the inner belt zone to be distinguished. An outer part, where the source seems to dominate, and in which the electron fluxes are enhanced during solar maximum, and an inner part, which is dominated by the losses, and which can be suppressed during solar maximum compared to solar minimum.

It must be noted, that the inner zone was for a longtime populated with high energy electrons which were injected from 1958-1962 by nucler explosions in the upper atmosphere [*Hess, 1968*]. As the lifetimes are long for MeV electrons trapped in the inner belt, this component decayed only slowly. Measurements of the inner belt electrons with instruments aboard CRRES in 1991 show, that the standard models, which are based on data of the 60's and early 70's, were probably still heavily contaminated by this artificial component and strongly overestimate the actual electron fluxes in the inner belt [*Abel et al., 1994*].

That the inner belt population, electrons and protons, can drastically change within a few minutes was demonstrated on March 24, 1991, when the interaction of a strong solar wind shock with the magnetosphere caused the creation of new radiation belts in the inner trapping zone [*Blake et al., 1992*]. The rapid compression of the magnetosphere during the associated Sudden Storm Commencement, SSC, induced an azimuthal electric field, which resonantly interacted with drifting particles of a limited energy range and transported them from beyond GEO down to L=2.5 [*Li et al. 1993, Hudson et al., 1995*]. Under conservation of the first adiabatic invariant the particles gained tens of MeV by the inward motion and formed long lasting new radiation belts in the inner trapping region.

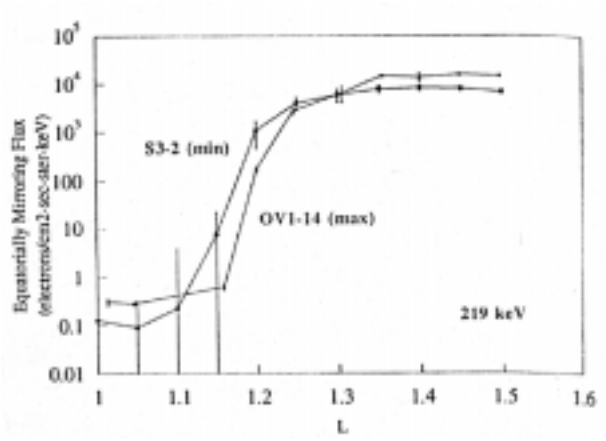

Figure 6: Comparison of inner belt electron radial profiles during solar maximum and solar minimum. There are two parts to be distiguished. An outer part, L>1.3 whichnis enhanced during solar maximum, and an inner part, L<1.3 where the which is enhanced during solar minimum (from Abel et al. [1994]).

4.2 Dynamics of the outer electron belt

Whereas the inner belt is subjected to slow variations, except during very strong geomagnetic events (see previous section), the outer electron belt is highly dynamic on shorter time scales. Figure 7 shows an L versus time count rate map of the >1 MeV electrons in a detector in GTO from August 1994 until August 1998. The lower panel shows the two day averaged count rates at L=4.5. The time series is characterized by a steady up and down with typical times scales of down to a fraction of a day. The variations are important. There is roughly a factor 1000 between the maximum and minimum fluence for an outer zone crossing observed during

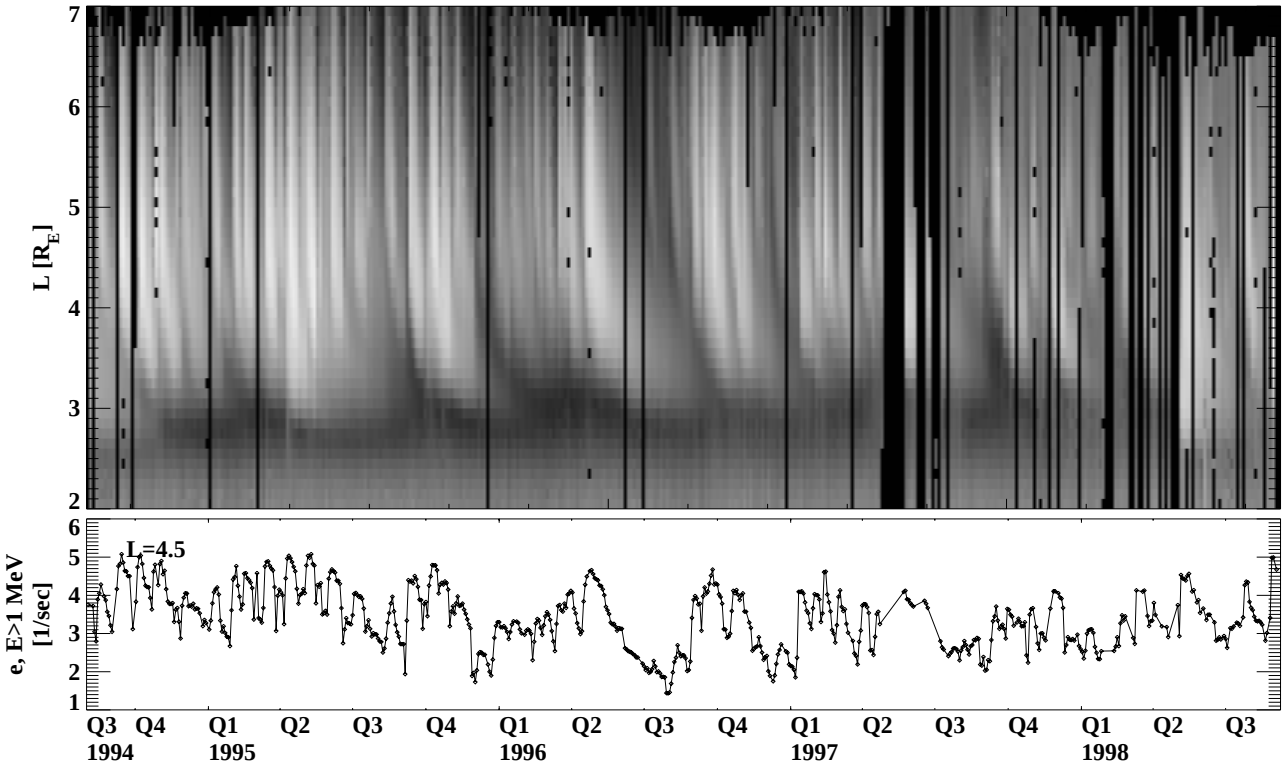

Figure 7: Illustration of the outer belt dynamiocs. the upper panel shows an L versus time map of the > 1 MeV count rates measured in GTO. Black regions mark missing data. The lower panel shows the temporal variations of the rates at L=4.5 R_E.

this period. Several quasi periodic variations of the high energy outer electron belt have been reported in the literature and can partly be seen also in figure 7. A solar cycle variation with maxima during solar maximum, semi-annual variation with maxima during spring and fall [*Desorgher et al., 1998*], variations with a period of 27 days, the solar rotation period [*Williams, 1966*].

Early is has been noted, that the variations are driven by the solar wind conditions. It is the interaction of fast solar wind streams with the magnetosphere which cause the fast changes. Figure 8 shows a typical sequence. The uppermost panel shows the solar wind speed measured aboard WIND as function of time and the second panel shows Dst. In this case the arrival of a fast solar wind stream in the evening of 28 January 1995 caused within the following day the build up of a moderate magnetic storm with minimum Dst of -50 nT, which only recovered slowly in the following days. The three panels in the third row show a series of radial >1 MeV electron count rate profiles for the same period measured in GTO. Three phases of variations can be noted. The first phase coincides with the storm main phase. During this phase the electron count rates decreased throughout the outer zone (profiles 1-3), however more significantly at larger L. The second phase started roughly one day after the arrival of the fast wind stream. Then the electron rates started to rapidly increase (profiles 4-7). Within one day they increased by a factor 10-100. Again the changes were most prominent at L-values between 4 and 6 R_E. The increase normally goes along with a hardening of the energy spectrum. It is first observed at low energies and then appears at higher energies. The third phase is characterized by slower variations. Until 6 February the electron count rates continued to slightly increase (profiles 8-12) but from then on slowly decayed again, until the arrival of the next fast solar wind stream initiated a similar sequence. All three phases are typical for the outer belt variations but their importance varies from event to event [*McIlwain, 1996*].

The coincidence of the initial decrease with the storm main phase suggests the ring current induced magnetic field changes to play an important role. In a first approximation the three adiabatic invariants can be considered to be conserved during the main phase field changes. In this case the magnetic field decrease causes a deceleration and an outward movement of the trapped particles. Both effects can contribute to the observed decrease. Since the energy spectrum of the electrons is steeply falling with higher energies, the deceleration causes less particles to be observed at a given energy [*Kim & Chan, 1997*]. This effect however is reversible. With the recovery of the magnetic field the particles are accel-

erated again. As there exist cases, where the electron levels do not recover to their prestorm values, real losses must also be involved. The outward movement of the particles can lead to such losses. Especially particles trapped at large L can be carried out to the magnetopause where they can be lost from stable trapping. Pitch angle scattering and precipitation may also contribute to the losses but have been shown not to be the dominating loss process during magnetic storms [*Imhof et al., 1991*].

The mechanisms which lead to the rapid increases is subject of intense research. Fast solar wind streams are the supposition. But although the solar wind drives the outer electron belt it is not the direct source of it. Although the energetic solar wind electrons could reach relativistic energies by radial diffusion into the trapping region, their number density is not sufficient to supply the outer belt [*Li et al. 1997*]. There is a tendency that the higher the wind speed, the larger the electron enhancement in the outer belt is. However, it has been noted that this relation is modified by the IMF orientation (promoted by southward IMF$_z$) [*Paulikas & Blake, 1979*] and also has a seasonal modulation with maximum efficiency during equinoxes [*Desorgher et al., 1998*]. It was also shown, that the enhancements mostly occur together with magnetic storms, but that the correlation between minimum Dst and maximum electron flux is poor [*Reeves, 1998*]. The fact, that the increases go together with a spectral hardening suggests the local energization of a lower energetic electron seed population to be responsible for the observed enhancements [*Baker et al., 1998a* and references therein, *Baker et al., 1998b*]. During substorms energetic electrons are injected from the tail region into the trapping region. They could provide the needed seed population. In this case substorm activity were one of the key features needed for the relativistic electron enhancements. There are several candidates for the acceleration process. In the past, normal radial diffusion and the so-called recirculation process were discussed [*Fujimoto & Nishida, 1990*], which although are probably in most cases to slow to account for the rapid increase. Rapid, shock driven radial diffusion, similar to the effect which has caused the creation of a trapped electron population in the inner belt region, but on smaller scales [*Li et al, 1998*], adiabatic acceleration due to the recovery of the magnetic field [*Bühler et al., 1998b*], or wave-particle interactions [*Summer et al., 1998, Boscher et al., 1998*] are other candidates, which all may contribute, with varying importance. Recently it was shown, that high energy electrons can also be trapped in the cusp region [*Sheldon et al., 1998*] and the possibility was discussed, that these electrons could feed the outer radiation belt [*Chen et al., 1998*].

During the third phase of variations, in which the electron belt changes slowly, radial diffusion and steady losses gain on importance again. The radial distribution moves inward and after a few days the electron rates start to decay again, similar to the evolution observed during geomagnetic quiet times.

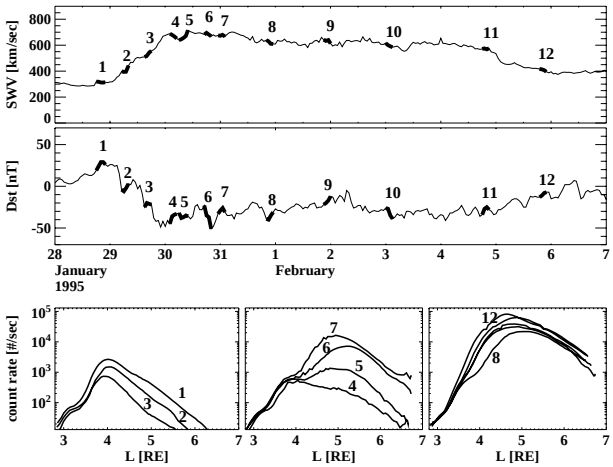

Figure 8: Outer radiation belt variations during a solar wind enhancement. In the upper two panels the solar wind speed (from WIND) and Dst are plotted versus time from January 28, 1995 to February 7, 1995. The lower three panels show radial electron profiles during the three phases of the outer belt variations (l.t.r.) phase one with rapid decay of the outer belt electron fluxes, phase two with rapid increase, and phase three with slow variations.

5. Final Remark

The radiation belts are variable with different typical time scales, reaching from minutes up to to years. Their proper modeling and forecasting is a challenging task within the "Space Weather" program.

References

Abel, B., Thorne, R.M., and Vampola, A.L., Solar cyclic behavior of trapped energetic electrons in earth's inner radiation belt, *J. Geophys. Res.* **99**, 19427, 1994

Albert, J.M., Ginet, G.P., and Gussenhoven, M.S., CRRES observations of radiation belt protons 1. Data overview and steady state radial disffusion, *J. Geophys. Res.* **103**, 9261, 1998

Baker, D.N., Li, X., Blake, J.B., and Kanekal, S., Strong electron acceleration in the earth's magnetosphere, *Adv. Space Res.* **21**, 609, 1998a

Baker, D.N., Pulkkinen, T.I., Li, X., Kanekal, K.W., Ogilvie, R.P., et al., A strong CME-related magnetic cloud interaction with the earth's magnetosphere: ISTP observations of rapid relativistic electron acceleration on May 15, 1997, *Geophys. Res. Lett.* **25**, 2975, 1998b

Blake, J.B., Kolasinski, W.A., Fillius, R.W., and Mullen, E.G., Injection of electrons and protons with energies of tens of MeV into L<3 on March 24, 1991, *Geophys. Res. Lett.* **19**, 821, 1992

Boscher, D., Bourdarie, S., Thorne, R., and Abel, B., Influence of the wave characteristics on the electron radiation belt distribution, *COSPAR*, **D05.0040**, Nagoya, 1998

Bühler, P., Desorgher, L., Zehnder, A., Daly, E., and Adams, L., Observations of the low earth radiation environment from Mir, *Radiat. Meas.* **26**, 917, 1996

Bühler, P., Desorgher, L., Zehnder, A., Daly, E., and Adams, L., REM measurements aboard Mir during 1995, *Adv. Space Res.* **21**, 1645, 1998a

Bühler, P., Johnstone, A. Desorgher, L. Zehnder, A., Daly, E., and Adams, L., The outer radiation belt during the 10 January, 1997 CME event, *Geophys. Res. Lett.* **25**, 2983, 1998b

Chen, J., Fritz, T.A., Sheldon, R.B., Spence, H.E. et al., Cusp energetic particle events: Implications for a major acceleration region of the magnetosphere, *J. Geophys. Res.* **103**, 69, 1998

Desorgher, L., Bühler, P., Zehnder, A., Daly, E., and Adams, L., Outer radiation belt variations during 1995, *Adv. Space. Res.* **22**, 83, 1998

Fujimoto, M. and Nishida, A., Energization and anisotropization of energetic electrons in the earth's radiation belts by the recirculation process, *J. Geophys. Res.* **95**, 4265, 1990

Gussenhoven, M.S., Mullen, E.G., and Violet, M.D., Solar particle events as seen on CRRES, *Adv. Space Res.* **14**, 619, 1994

Hess, W.N., The earth's radiation belt, *Handbuch der Physik* **XLIX/4**, 115, 1968

Hudson, M.K., Kotelnikov, A.D., Li, X., Roth, I., and Temerin, M., Simulation of proton radiation belt formation during March 24, 1991 SSC, *Geophys. Res. Lett.* **22**, 291, 1995

Hudson, M.K., Marchenko, V.A., Roth, I., Temerin, M., Blake, J.B., and Gussenhoven, M.S., Radiation belt formation during storm sudden commencement and loss during main phase, *Adv. Space Res.* **21**, 597, 1998

Huston, S.L. and Pfitzer, K.A., A new model for the low altitude trapped proton environment, *IEEE Nucl. Sci. Rad. Effects Conference*, July, 1998

Imhof, W.L., Voss, H.D., Mobilia, J., Datlowe, D.W., McGlennon, J.P., and Baker, D.N., Relativistic electron enhancements: simultaneous measurements from synchronous and low altitude satellites, *Geophys. Res. Lett.* **18**, 397, 1991

Kim, H.-J. and Chan, A.A., Fully adiabatic changes in storm time relativistic electron fluxes, *J. Geophys. Res.* **102**, 22107, 1997

Lencheck, A.M. and Singer, S.F., Effects of finite gyroradii of geomagnetically trapped protons, *J. Geophys. Res.* **67**, 4073, 1962

Li, X., Roth, I., Temerin, M., Wygant, J.R., Hudson, M.K., and Blake, J.B., Simulation of the prompt energization and transport of radiation belt particles during the March 24, 1991 SSC, *Geophy. Res. Lett.* **20**, 2423, 1993

Li, X., Baker, D.N., Temerin, M., Larson, D., Lin, R.P., Reeves, G.D., Looper, M., Kanekal, S.G., and Mewaldt, R.A., Are energetic electrons in the solar wind the source of the outer radiation belt?, *Geophys. Res. Lett.* **24**, 923, 1997

Li, X., Baker, D.N., Temerin, M., Cayton, T., Reeves, G.D., Araki, T., Singer, H., Larson, D., Lin, R.P., and Kanekal, S.G., Energetic electron injections into the inner magnetosphere during the Jan. 10-11, 1997 magnetic storm, *Geophys. Res. Lett.* **25**, 2561, 1998

Lyons, L.R. and Thorne, R.M., Equilibrium Structure of radiation belt electrons, *J. Geophys. Res.* **78**, 2142, 1973

McIlwain, C.E., Coordinates for mapping the distribution of magnetically trapped particles, *J. Geophys. Res.* **66**, 3681, 1961

McIlwain, C.E., Processes acting upon outer zone electrons, *Geophys. Monograph Series* **97**, 15, 1996

Northrop, T.G. and Teller, E., Stability of the adiabatic motion of charged particles in earth's field, *Phys. Rev.* **117**, 215, 1960

Paulikas, G.A. and Blake, J.B., Modulation of trapped energetic electrons at 6.6 R_E by the direction of the interplanetary magnetic field, *Geophys. Res Lett.* **3**, 277, 1976

Reeves, G.D., Relativistic electrons and magnetic storms: 1992-1995, *Geophys. Res. Lett.* **25**, 1817, 1998

Sawyer, D.M. and Vette, J.I., AP8 trapped proton environment for solar maximum and solar minimum, *NSSDC/WDC-A-R&S 76-06*, 1976

Selesnick, R.S., Blake, J.B., Kolasinski, W.A., and Fritz, T.A., A quiescent state of 3 to 8 MeV radiation belt electrons, *Geophys. Res. Lett.* **24**, 1343, 1997

Schulz, M. and Lanzerotti, L.J., Particle diffusion in the radiation belts, Springer-Verlag, 1974

Sheldon, R.B., Spence, H.E., Sullivan, J.D., Fritz, T.A., and Chen, J., The discovery of trapped energetic electrons in the outer cusp, *Geophys. Res. Lett.* **25**, 1825, 1998

Stoermer, C., *Arch. Sci. Phys. Nat.* **24**, 317, 1907

Summer, D., Thorne, R.M., and Xiao, F., Relativistic theory of wave-particle resonant diffusion with application to electron acceleration in the magnetosphere, *J. Geophys. Res.* **103**, 20487, 1998

Vette, J.I., The AE8 trapped electron environment, *NSSDC/WDC-A-R&S 91-24*, 1991

Williams, J., A 27-day periodicity in outer zone trapped electron intensities, *J. Geophys. Res.* **71**, 1815, 1966